11-8-2000

The Effectiveness of the ASOS, MMTS, Gill, and CRS Air Temperature Radiation Shields*

K. G. Hubbard
University of Nebraska-Lincoln, khubbard1@unl.edu

X. Lin
University of Nebraska-Lincoln

E.A. Walter-Shea
University of Nebraska - Lincoln

The Effectiveness of the ASOS, MMTS, Gill, and CRS Air Temperature Radiation Shields*

K. G. HUBBARD, X. LIN, AND E. A. WALTER-SHEA

School of Natural Resource Sciences, University of Nebraska—Lincoln, Lincoln, Nebraska

(Manuscript received 13 June 2000, in final form 8 November 2000)

ABSTRACT

Periodic upgrades of air temperature measurement systems in surface weather station networks cause data discontinuities. From a climatological viewpoint, it is necessary to evaluate the air temperature data discontinuities when air temperature radiation shields are upgraded. This study was undertaken to investigate the effectiveness of four common air temperature radiation shields including the Automated Surface Observing System (ASOS), the Maximum–Minimum Temperature System (MMTS), the Gill, and the Cotton Region Shelter (CRS) shields. The solar radiation shielding effectiveness for each shield under typical grass ground surface and different artificial surfaces (black, white, and aluminum) were investigated. The shield effectiveness was evaluated by measuring the interior solar irradiance and the inner surface temperatures of radiation shields. Parabolic curves describe the fraction of solar radiation entering shields, which increased as the solar reflectivity of the underlying surface increased. The rank of solar radiation shield effectiveness was ASOS > CRS > MMTS > Gill (i.e., total interior solar irradiance loading in relative terms was ASOS:CRS:MMTS:Gill = 1:1.3:1.7:2.5), under typical grass surface conditions. The increase in interior solar irradiance from the typical grass surface to the white surface went up by a factor of 1.2, 2.3, 1.6, and 1.9, respectively, for the ASOS, MMTS, Gill, and CRS shields. The ASOS shield had an obvious drawback for the infrared radiation effectiveness due to using the chilled mirror heating/cooling system as the dewpoint temperature measuring system located in the middle portion of the shield. The rank of the infrared radiation shielding effectiveness was CRS > MMTS > Gill > ASOS during daytime and Gill ≥ MMTS > CRS ≈ ASOS during nighttime.

1. Introduction

Outdoor air temperature observation systems commonly shield the air temperature sensor from solar radiation. Ideally, the shield prevents the sun's direct rays and reflected solar rays from heating the sensor, shelters the sensor from inclement weather, and allows adequate airflow to ventilate the sensor. Advances in temperature sensor technology have led to air temperature sensors with accuracies of ±0.01°–±0.02°C in controlled conditions (Hart Scientific, Inc. 1996). However, in the field, it has been impossible to achieve such high accuracy because air temperature radiation shields cannot completely block solar radiation without retarding natural airflow. The lack of ventilation causes inadequate coupling of sensor and air temperature, the greatest source of error in air temperature measurements (Brock et al. 1995). With adequate airflow, air temperature sensors tend to stay in thermal equilibrium with the air. While forced ventilation ensures adequate airflow, it is not feasible in remote locations where power (alternating current) is not available.

The commonly used shields today are the Cotton Region Shelter (CRS), the Maximum–Minimum Temperature System (MMTS) shield, the Gill shield, and the Automated Surface Observing System (ASOS) shield. The CRS was used in the United States for many decades as the principal air temperature shield. This wooden structure has adequate space to house maximum and minimum liquid-in-glass (LIG) thermometers. In some cases, a bimetallic thermograph was placed in the CRS to record continuous air temperature. With the advent of sensor technology, air temperature sensors became smaller and easier to interface, thus eliminating the need for large shields like the CRS. In the mid- to late-1980s, the MMTS, with a multiple stacked-plate design, began replacing the CRS in the U.S. cooperative weather station network. The MMTS shield contains a thermistor from which the daily maximum and minimum air temperatures are displayed on an MMTS readout. The Gill shield is a multiple-plate cylindrical shaped shield (Gill 1979) that has been widely used in nonfederal automated weather station networks. The ASOS was planned and installed in the early 1990s. The air temperature and dewpoint temperature measuring system used in the ASOS consists of a platinum-wire resis-

* Nebraska Agriculture Experiment Station Journal Number 13013.

Corresponding author address: Prof. Kenneth G. Hubbard, School of Natural Resource Sciences, University of Nebraska—Lincoln, 242 L. W. Chase Hall, Lincoln, NE 68583-0728.
E-mail: khubbard@unl.edu

TABLE 1. Geometrical dimensions of the CRS, Gill, MMTS, and ASOS shields.

Shields	CRS (mm)	Gill (mm)	MMTS (mm)	ASOS (mm)
Shield height	830	158	240	390
Width × depth or diameter	765 × 515	120	235	112
Airflow gap height	15–12	13	25.4	Closed
Central open space	All[a]	127[b] × 32[c]	150[b] × 85[c]	Part[d]
Sensor's height[e]	150–250	70–85	95–115	50–80

[a] All space inside the CRS is open.
[b] The central open space height of the inner cylinder inside the shield.
[c] The central open space diameter of the inner cylinder inside the shield.
[d] Only a small part of the open space is for the temperature sensor in the ASOS.
[e] Heights subtended by the sensors in normal operating conditions.

tance temperature (PRT) sensor to measure air temperature and a chilled mirror to measure dewpoint temperature. The PRT is located in a cylindrical-shaped, metal shield in the stream of air that enters through a circular opening at the base of the shield. The geometrical dimensions are shown in Table 1 for these four commonly used air temperature radiation shields.

Daytime heat loading on a sensor depends mainly on incoming global solar radiation and solar radiation reflected by the underlying surface, but the difference in

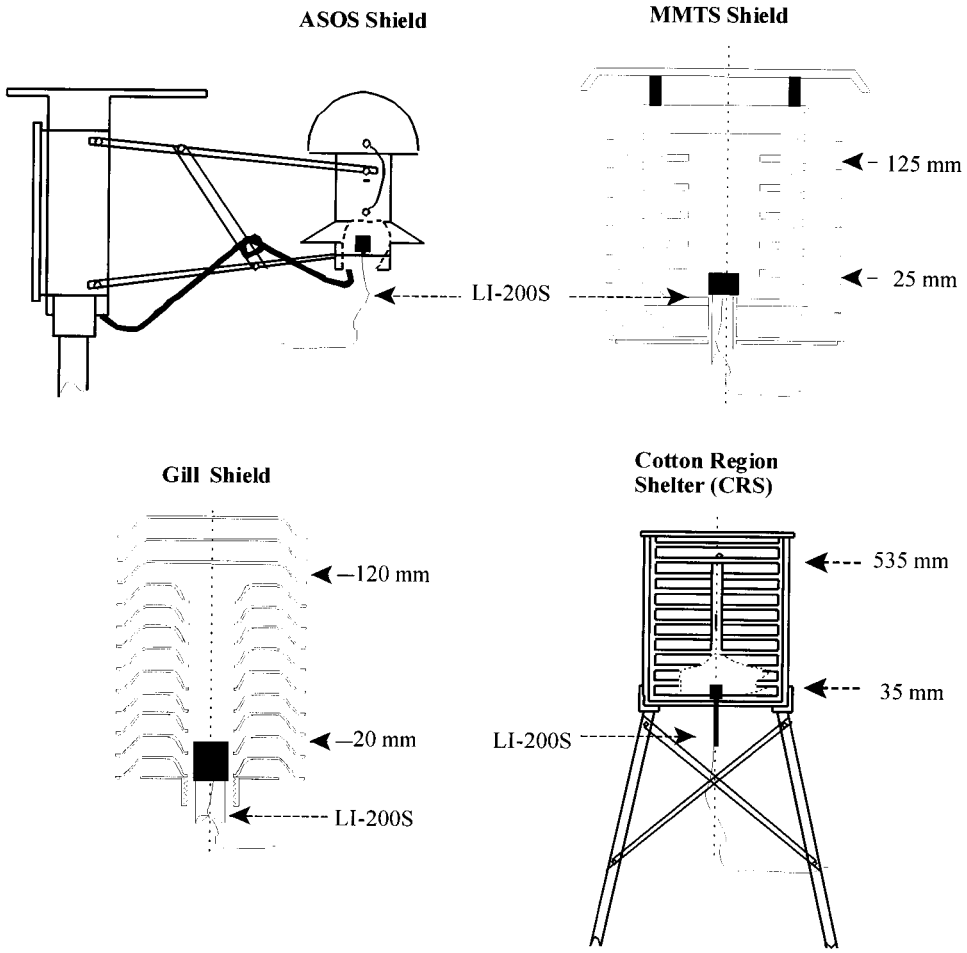

FIG. 1. Sketch of LI-200S pyranometer locations inside the shields. The ASOS shield provides only one position to install the LI-200S. There are six positions available inside the MMTS, Gill, and CRS shields. Both the lowest and highest positions are labeled on each shield. The other four measurement positions are located between the lowest and highest position with equal distance. Note that the four shields above are not under the same scaling size.

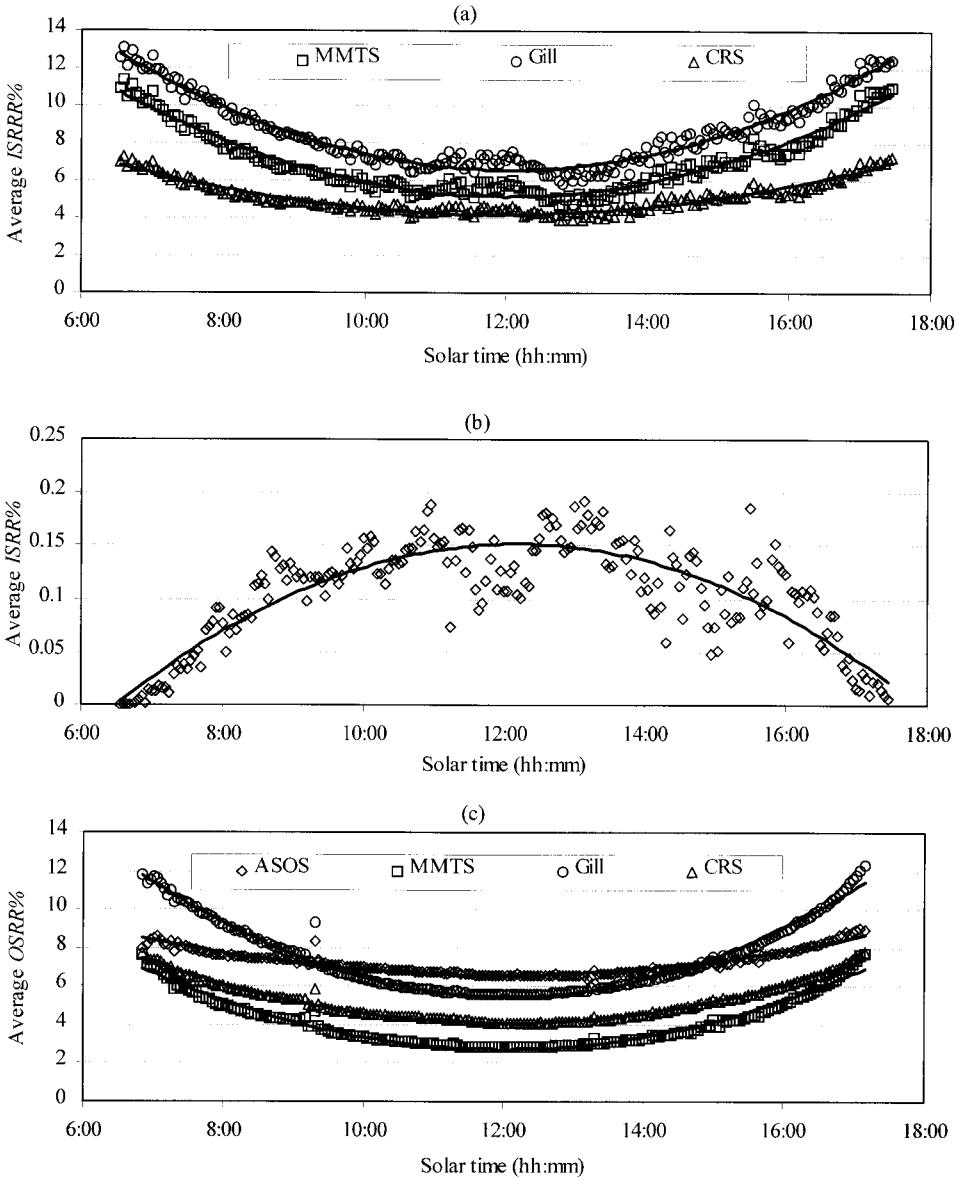

FIG. 2. (a) Average ISRR% of six height measurements inside the MMTS, Gill, and CRS shields. (b) Average ISRR% of six daytime measurements inside the ASOS shield. (c) Average OSRR% of four height measurements for the MMTS, Gill, and CRS shields and average OSRR% for four daytime measurements (one height) inside the ASOS shield.

TABLE 2. The regression coefficients of Eq. (3) for the ISRR%, OSRR%, and TSRR% inside each radiation shield. The r^2 represents the regression coefficient of determination.

	ISRR%			OSRR%			TSRR%		
Shields	*a*	*b*	r^2	*a*	*b*	r^b	*a*	*b*	r^2
ASOS	0.152	−0.0047	0.72	6.569	0.076	0.93	3.364	0.0357	0.91
MMTS	5.136	0.186	0.95	2.701	0.159	0.98	4.272	0.179	0.95
Gill	6.562	0.205	0.96	5.458	0.232	0.98	6.834	0.236	0.96
CRS	4.178	0.0092	0.92	4.085	0.126	0.99	4.452	0.106	0.95

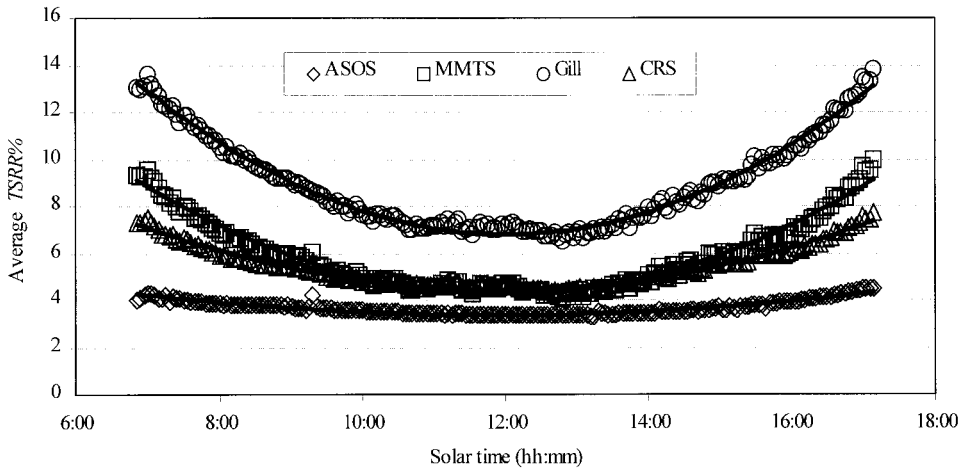

FIG. 3. Average TSRR% for the ASOS, MMTS, Gill, and CRS shields. The integrated area of each curve from solar time 0600–1800 is 45.5, 77.0, 115.9, and 68.6, respectively, for the ASOS, MMTS, Gill, and CRS shields.

air and sensor temperatures is reduced at higher ambient wind speeds (McKay and McTaggart-Cowan 1977; Gill 1983; Wylie and Lalas 1992; Wendland and Armstrong 1993; Richardson 1995; Guttman and Baker 1996). An ideal radiation shield would block all solar radiation; however, this is currently impossible because openings are necessary to allow airflow through the shield. Therefore, the determination of interior solar radiation becomes necessary to evaluate the effectiveness of the radiation shields. Gill (1983) conducted wind tunnel tests of several naturally ventilated radiation shields under high radiation and low wind speed conditions. An array of high output lamps was used to simulate the sun, and the shield was placed over a simulated snow surface. The air temperature error varied greatly depending on wind speed and shield type, ranging from +5° to nearly +20°C at the lowest wind speeds. In addition, when the temperatures of the sensor and the interior walls are not equal there is a net exchange of infrared radiation, and the sensor temperature will no longer represent the ''air'' temperature.

Fuchs and Tanner (1965) investigated the performance of various shield coatings with respect to radiative characteristics for solar and thermal radiation. The results indicated that coatings with a small ratio of solar absorptivity to infrared absorptivity were best for solar radiation shields, particularly when they were resistant to weathering. Gill (1979) pointed out that ''the degree of heating in full sun is of primary importance to choice of materials, and the nocturnal radiation characteristics only secondary.'' The multiple-plate radiation shields (e.g., Gill shield) usually have air temperature errors of about 0.5°–1°C (Richardson 1995) but sometimes reach nearly 2.0°C (Tanner et al. 1996) during the daytime.

Thus, the radiation incident on the air temperature sensor is composed of two main components, scattered solar radiation and infrared radiation. Both solar radiation and infrared radiation affect the air temperature accuracy in the measurements since any radiation shield will have a nonperfect reflectivity and a nonzero absorptivity. Measurements of the solar radiation penetrating the interior of the shield and the infrared radiation emitted by the inside walls of the shield provide a means of quantifying the shield effectiveness.

Historical climate periods can be characterized by the type of radiation shields in use. A change from one type of shield to another causes systematic changes in the air temperature biases. Thus, it is necessary to evaluate radiation shield differences to understand the contributing causes and to eventually, or potentially, correct for the ''shield'' bias present in data from existing weather station networks. The specific objective of this study is to investigate the effectiveness of four common radiation shields. To accomplish this the following aspects were quantified: 1) the solar irradiance inside the ASOS, the MMTS, the Gill, and the CRS radiation shields; 2) solar irradiance changes inside the shields when the underlying surface is changed; and 3) the temperature difference between the inner-wall temperature of the radiation shield and the sensor temperature.

2. Materials and methods

a. Experimental design and measurements

Solar irradiance inside the shields was measured during the summer of 1998 at the University of Nebraska's Horticulture Experimental Site (40°83′N, 96°67′W, altitude 383 m) located in Lincoln, Nebraska. This site is on flat terrain with a surface of mowed grass. There are few physical obstructions within a radius of 100 m and none within 25 m. Ambient global solar irradiance was measured at a distance 20 m from the radiation shields at a height of 1.5 m. The ASOS, MMTS, Gill, and CRS

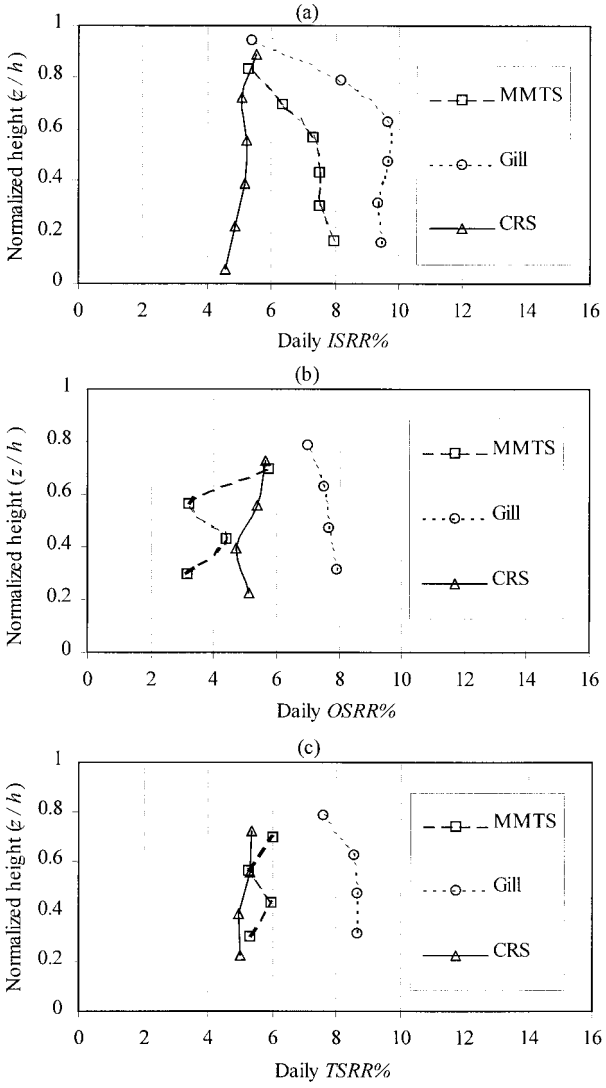

FIG. 4. Profiles of (a) daily ISRR%, (b) daily OSRR%, and (c) daily TSRR% inside the MMTS, Gill, and CRS shields. Note that there are no profiles inside the ASOS shield due to the limited inner space of the ASOS shield. All daily values were taken from 0700–1700 solar time.

shields were mounted at a height of 1.5 m above the grass surface and 10 m apart. A calibrated pyranometer [model LI-200S (LI-COR, Inc., 1991)] was mounted inside each of the four radiation shields to measure the solar irradiance (see appendix for calibration details). The interior space of the ASOS radiation shield is limited due to the aspirator fan and hygrothermometer assembly enclosed in the ASOS system, so the LI-200S was mounted at the air temperature sensor height (Fig. 1). The LI-200S was positioned at each vertical height in the center of the shields from 25 mm (H1) to 125 mm (H6) at 20-mm intervals for the MMTS shield, from 20 mm (H1) to 120 mm (H6) at 20-mm intervals for the Gill shield, and from 35 mm (H1) to 535 mm (H6) with 100-mm intervals for the CRS shield. At each height, the upward solar irradiance was measured. The downward irradiance was measured at four vertical heights (H2–H5) because the LI-200S pyranometer could not be mounted at either the highest position (H6) or the lowest position (H1). The normal operating heights subtended by the air temperature sensors in the radiation shields are from 85 to 105 mm for the MMTS, from 60 to 85 mm for the Gill (depending on the sensor's dimension and the user's installation), and from 110 to 155 mm for the CRS shield [i.e., the standard LIG thermometer position in the CRS (Meteorological Office 1965)]. The pyranometer was attached with silicon adhesive to a white PVC tube (22 mm in outer diameter), which slid up and down to the desired heights within the shields (except for the ASOS shield). During the measurements, the radiation shields and pyranometers were kept level.

Contributions of solar irradiance from underlying ''artificial'' surfaces were measured inside the shields with the LI-200S installed at the normal operating air temperature sensor height. An artificial ground surface was created by installing first aluminum, then black, and finally white painted plywood over a rectangular area 7.32 m $\times$ 4.88 m. The natural grass surface and the three painted plywood surfaces gave four surface treatments. Surface solar reflectivities (daily average) are 0.06, 0.24, 0.69, and 0.85 for the black, grass, aluminum, and white surfaces, respectively (Monteith and Unsworth 1990; Lin and Hubbard 1999). Above each surface treatment, the radiation shields were installed at 1.5 m at symmetrical positions (separation distance was 2.44 m) along the center line length of the artificial surface. Incoming solar irradiance (with the pyranometer installed facing upward) and outgoing solar irradiance measurements (with the pyranometer inverted) were measured inside the ASOS, MMTS, Gill, and CRS shields under clear sky conditions. To maintain accuracy the same combination of components were used in the field as in the calibration process [i.e., the same CR10 datalogger, the same wiring for the pyranometers, high-resolution mode, data sampling (5 s), and averaging time interval (3 min)]. The duration of solar irradiance measurements was from 20 June to 30 September (DOY 171 to DOY 273, 1998). The criteria for selecting the data for analyses were based on weather conditions; that is, only cloudless daytime or mostly sunny daytime data were used to evaluate the solar irradiance inside the shields. All solar irradiance measurements were collected corresponding to solar time.

Infrared radiation effects on air temperature measurements were determined using the difference between the shield's average inner-surface (wall) temperature and the sensor temperature. Five fine-wire Cement-On thermocouples (Type E, 1.27 mm in thickness, 9 mm $\times$ 19 mm rectangle shape) were installed on the inner surfaces of each shield located above, east, south, west, and north of the air temperature sensor to measure the inner-surface temperatures of

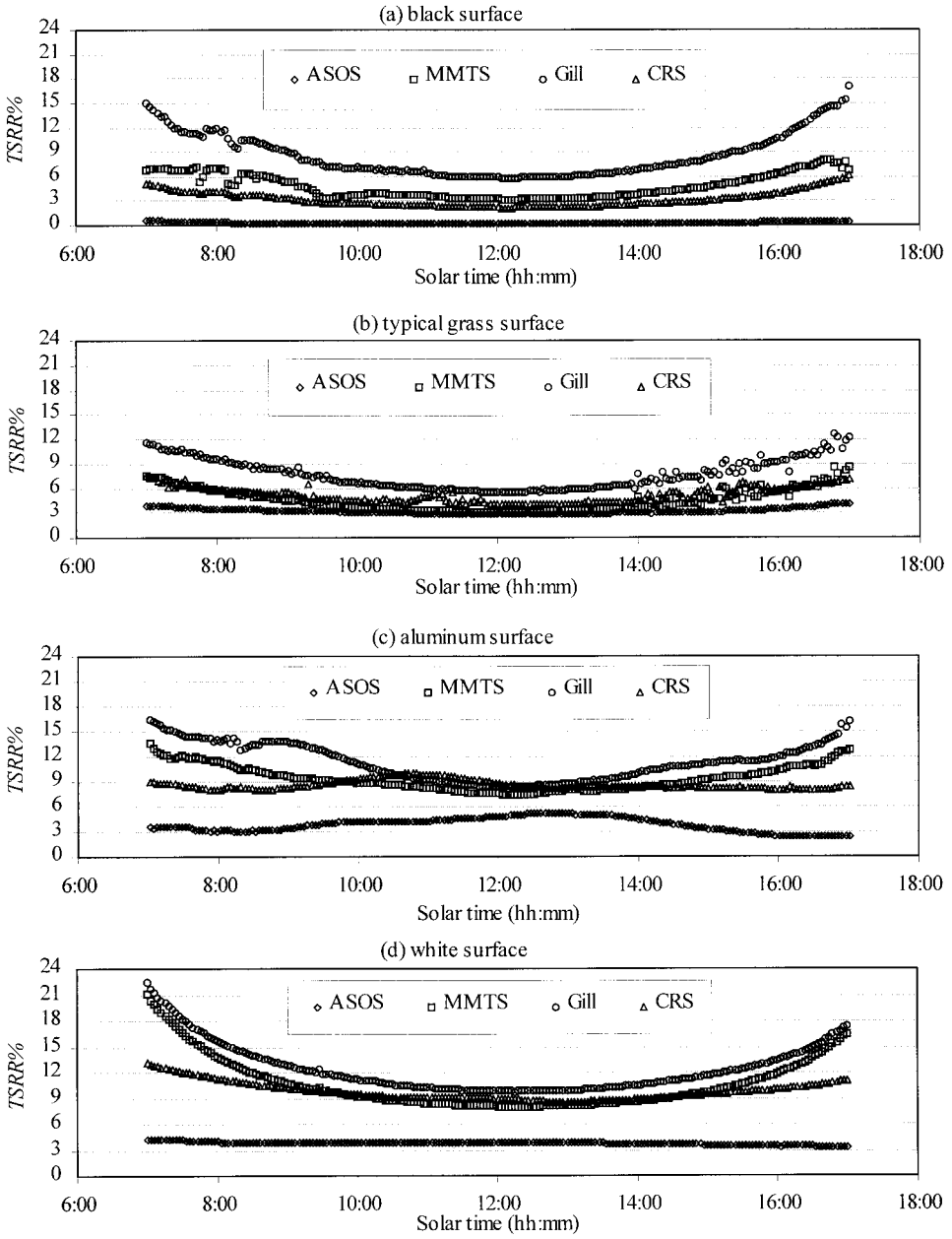

FIG. 5. TSRR% at the air temperature sensor positions in the radiation shields exposed to different underlying surfaces [(a) black surface, (b) typical grass surface, (c) aluminum surface, and (d) white surface].

each shield. The inner-surface thermocouples were in full view of the air temperature sensor inside the shield but did not cause an obstruction to airflow or solar irradiance. The temperature sensors inside the shields were the hygrothermometer inside the ASOS, the thermistor inside the MMTS, the HMP35 (Vaisala, Inc.) air temperature and relative humidity sensor inside the Gill, and the HMP35 sensor inside the CRS shield. All thermocouples were calibrated using a dry-well temperature calibrator, Model D55SE (AMETEK, Inc., JOFRA Instruments) with ± 0.3°C accuracy. Both inner surface (wall) thermocouples and air (sensor) temperatures were measured from January to October 1997 at the experimental site. The inner surface thermocouples were recalibrated once during the measurement period. The sampling frequency for the inner surface temperature and the air temperature sensor measurements was 30 min.

b. Data analysis

The relative magnitude of incoming solar irradiance inside each shield is evaluated using the term incoming solar radiation ratio (ISSR%), defined as

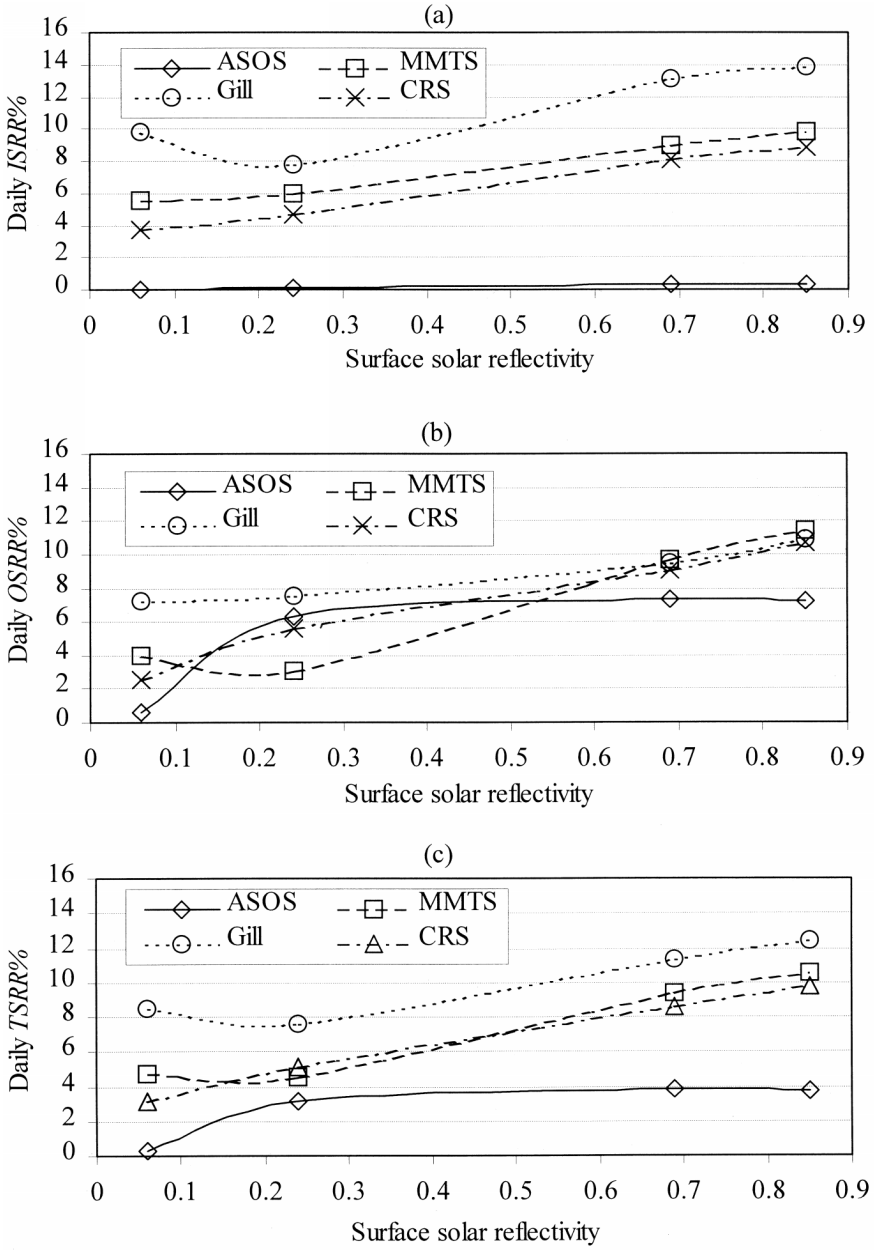

FIG. 6. (a) Daily ISRR%, (b) daily OSRR%, and (c) daily TSRR% changes with changes of underlying surface solar reflectivity.

$$\text{ISRR\%} = \frac{\text{Incoming solar irradiance inside shield}}{\text{Incoming global solar irradiance outside shield}} \times 100. \quad (1)$$

The numerator on the right-hand side of Eq. (1) is the incoming solar irradiance inside the shield measured when the LI-200S is mounted facing upward. Likewise, the outgoing solar radiation ratio (OSRR%) is defined the same as (1) except that the numerator of the right-hand side of (1) is the outgoing solar irradiance inside the shield (i.e., when the LI-200S is mounted facing downward).

Total solar radiation (TSRR%) loading can be calculated by combining the contributions of ISRR% and OSRR% as

$$\text{TSRR\%} = 0.5(\text{ISRR\%} + \text{OSRR\%}). \quad (2)$$

''Averages'' of ISRR%, OSRR%, and TSRR% were calculated as the mean ratio over all heights for each given time and shield. ''Daily'' ISRR%, OSRR%, and TSRR% were defined as the mean ratio over the day at a specific height. When the vertical profile of the daily

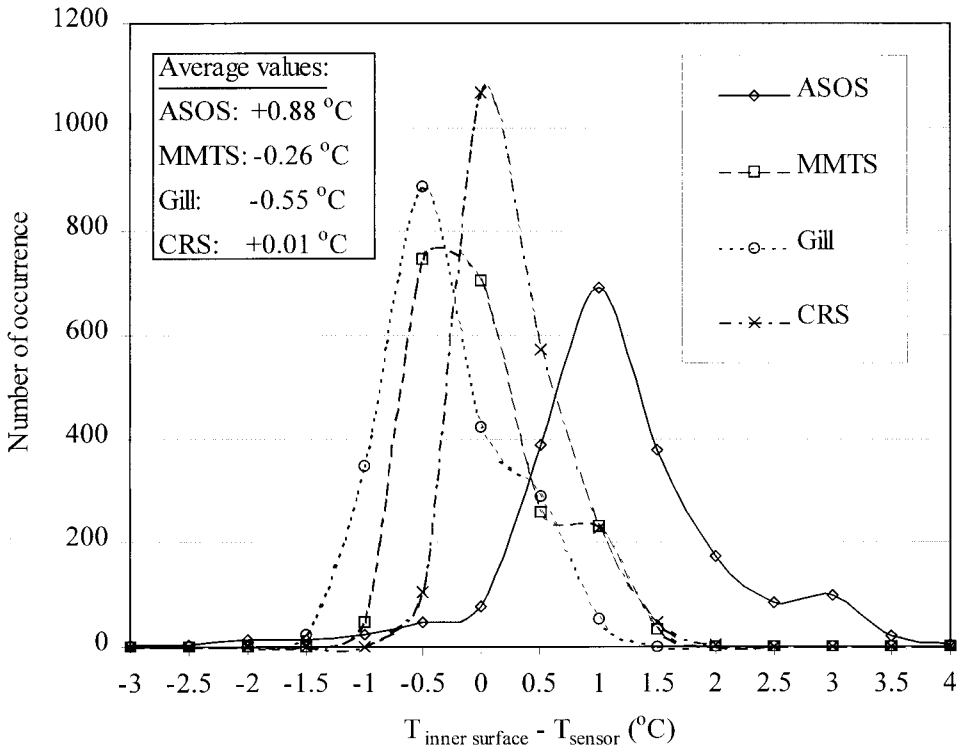

FIG. 7. Temperature differences between the average inner-surface temperature of the shields and the normal operating sensor temperature inside the shield during the daytime. The total data numbers are 2025 observations taken in 1997, from DOY 15 to DOY 39, DOY 121 to DOY 157, and DOY 210 to DOY 232.

solar radiation ratio was examined, the heights in the shields were normalized by the total open space height. The normalized heights (z/h, where z represents the height of measurement and h refers to interior vertical extent of the open space) of the sensors during the normal operations were approximately 0.6–0.79 for the Gill, 0.57–0.70 for the MMTS, and 0.18–0.25 for the CRS.

The ISRR%, OSRR%, and TSRR% for the radiation shields were expressed as nonlinear (parabolic) functions of solar time during daylight hours of the general form

$$\text{ratio\%} = a + bt^2. \tag{3}$$

Mathematically, Eq. (3) represents a standard parabolic curve, where ratio% refers to either ISRR%, OSRR%, or TSRR%, and t represents the solar time (a shift of 12 h is used so that at solar noon the equation reaches a minimum or maximum, i.e., t = solar time − 12). The parameter a represents the minimum ratio% incident on the air temperature sensor inside the ASOS, Gill, MMTS, and CRS shields. The parameter b in Eq. (3) denotes the degree of openness of the parabola. As b becomes smaller, the parabola becomes more open and is flat when $b = 0$. Therefore, the integration area of parabolic curve was taken as an indication of solar shielding effectiveness for each radiation. The incoming solar irradiance inside the radiation shield was measured on six nearly consecutive clear sky days. Each day data were collected from a different height within the shield. DOY 183, 184, 185, 179, 181, and 182 in 1998 correspond to the heights H1–H6. The outgoing solar irradiance was selected from four clear days, with data collected from a different height within the shield on each day. DOY 208, 230, 220, and 229 in 1998 correspond to the heights H2–H5.

The five inner surface temperatures were simply averaged to represent the shield inner surface temperature. The inner surface temperature data for 85 days were taken from DOY 15 to 39, from DOY 121 to 157, and from DOY 210 to 232, 1997. The difference between the average inner surface temperature and the sensor temperature is used to evaluate the infrared shielding effectiveness for each radiation shield.

3. Results

a. The solar radiation environment inside the shields

Average ISRR% for the MMTS, Gill, and CRS decreased in value with increasing solar elevation angle (Fig. 2a). The ISRR% inside the ASOS (one height) followed the opposite trend (Fig. 2b) owing to the fact that the bottom of the ASOS shield is essentially open toward the ground surface and covered only by a metal mesh. The coefficients a and $b$were found by nonlinear

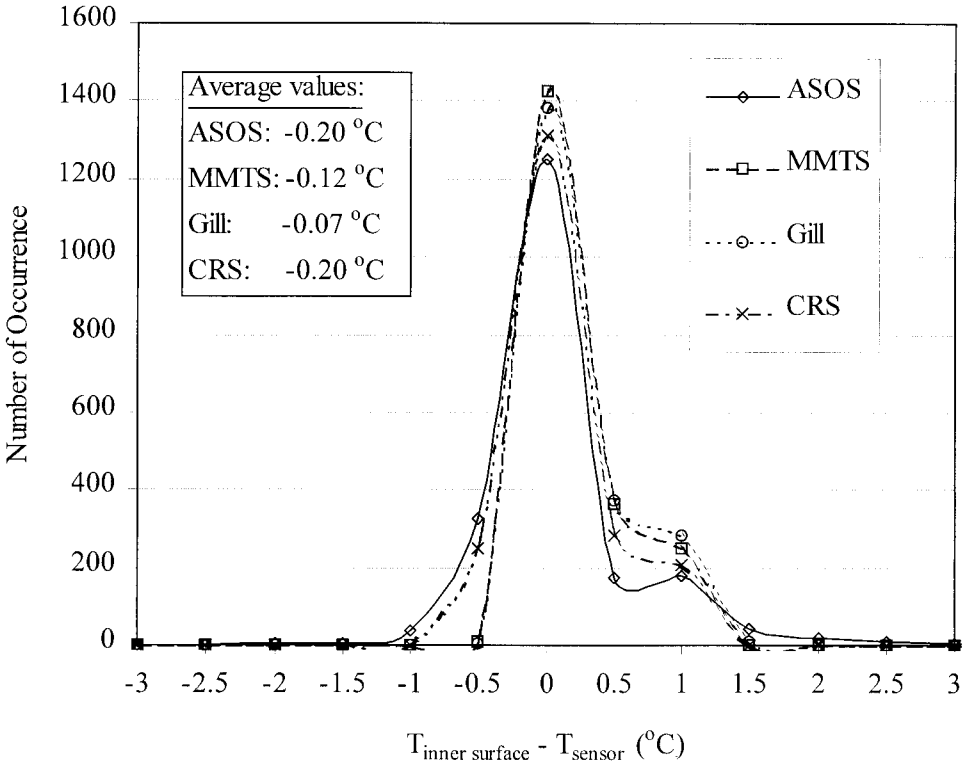

FIG. 8. Temperature differences between the average inner surface temperature of the shields and the normal operating sensor temperature inside the shield during nighttime. The total data number are 2053 observations taken in 1997, from DOY 15 to 39, DOY 121 to DOY 157, and DOY 210 to DOY 232.

regression (Table 2). Based on the integration area under the curve, the ISRR% ranks as follows: Gill > MMTS > CRS > ASOS (Figs. 2a,b).

The trends in average OSRR% over four measurement heights for the MMTS, Gill, and CRS (Fig. 2c) followed similar trends as for the average ISRR%, while the trends for the ASOS's average OSRR% was the opposite of the ASOS's average ISRR% attributed to the open bottom of the ASOS shield (Fig. 2). Again, coefficients for Eq. (3) were determined and the area under the curve was determined by integration. This revealed that the OSRR% ranks as follows: Gill > ASOS > CRS > MMTS.

The trend in the average TSRR% inside the shields followed the sum of average ISRR% and average OSRR% (Fig. 3). Similarly, based on the integration areas, the TSRR% (Table 2 and Fig. 3) had the following relative magnitudes: ASOS:MMTS:Gill:CRS = 1:1.7:2.5:1.3 (45.5:77.0:115.9:68.6).

The profiles of daily ISRR%, OSRR%, and TSRR% demonstrated that the daily ISRR% (Fig. 4a) was largest at the middle position of the Gill shield and at the bottom position of the MMTS shield. The daily ISRR% of the CRS shield was quite consistent from the bottom to the top. The daily OSRR% (Fig. 4b) for the MMTS fluctuated and was smallest compared to the other two shields. The Gill shield had the largest OSRR% over all heights. The TSRR% at each height inside the Gill, MMTS, and CRS shields (Fig. 4c) illustrates that the MMTS's daily TSRR% was nearly the same as for the CRS (between 5% and 6%), while the daily TSRR% for the Gill shield remained the largest.

b. Solar irradiance inside the shields over surfaces with different solar reflectivities

As the underlying surface solar reflectivity increased with changes from black, to grass, to aluminum, and then to white surface, the interior solar radiation generally increased. The trends in TSRR% with time were generally the same from one surface to another, with the exception of ASOS and CRS above aluminum (Fig. 5). For the black surface, the TSRR% had distinct differences among the Gill, MMTS, CRS, and ASOS shields (Fig. 5a). Above the highly reflective white surface, the TSRR% of the Gill, MMTS, and CRS shields were the highest encountered.

Increasing the solar reflectivity from a black to a white surface for the ASOS had little effect on the daily ISRR%, due to the solid barrier represented by the ASOS structure and the black painted inner surface (Fig. 6a). The daily ISRR% inside the Gill, MMTS, and CRS had almost the same linear increasing rate with the increase of surface solar reflectivity. The daily

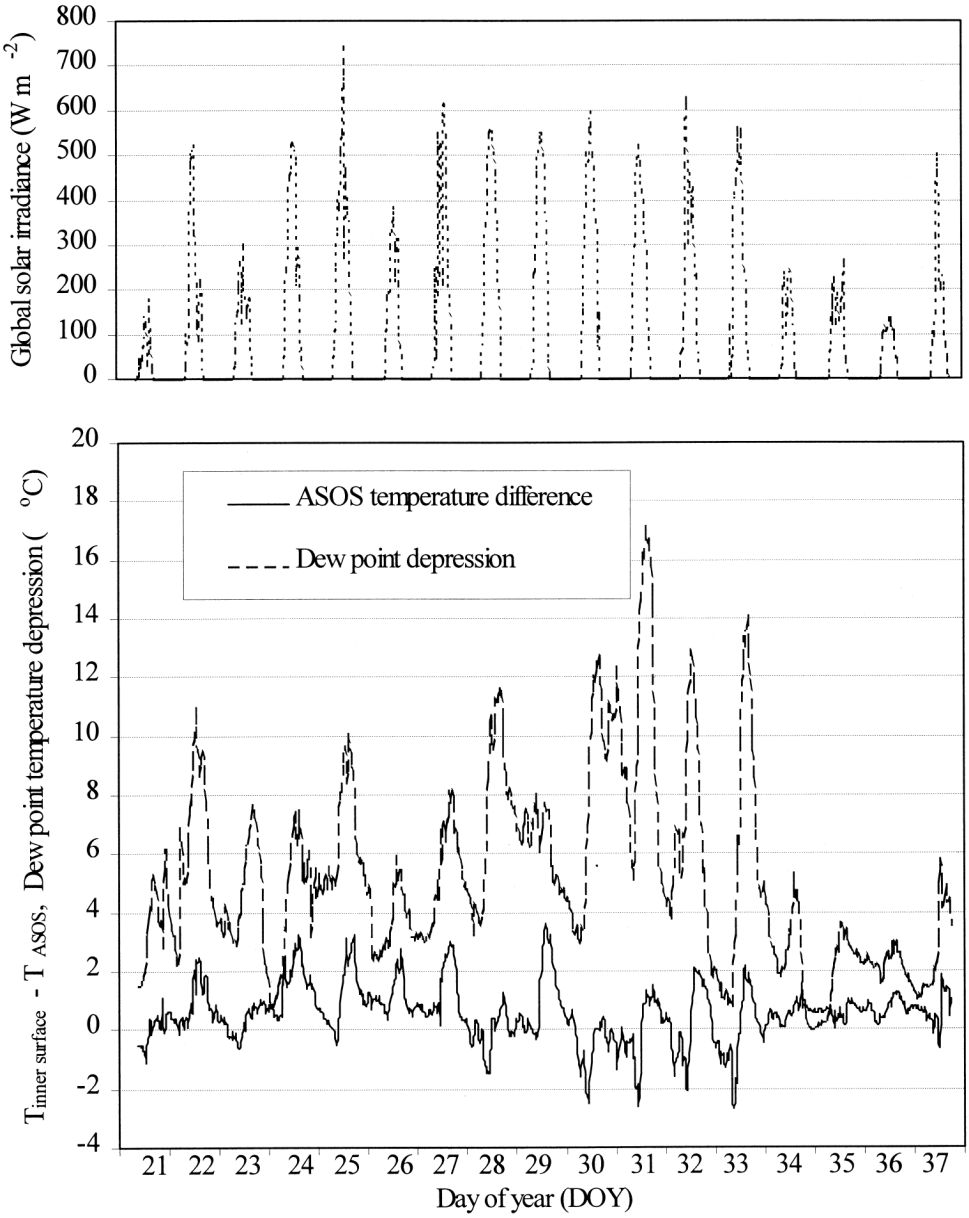

FIG. 9. (bottom) ASOS temperature difference between the inner surface temperature of the ASOS shield ($T_{\text{inner surface}}$) and the ASOS sensor temperature reading (T_{ASOS}), and dewpoint temperature depression, and (top) global solar irradiance, from CST 0900 of DOY 21 to 1800 of DOY 37, 1997.

OSRR% trends inside the shields were different from that of the ISRR% (Fig. 6b). The OSRR% for the ASOS increased as the reflectivity changed from the black to the grass surface and remained almost constant (around 7.5%) for surface solar reflectivity of 0.25 and above. This result is attributed to the fact that the black inner surface of the ASOS shield absorbs the reflected solar radiation from the ground surface. The daily OSRR% of the CRS and MMTS increased more rapidly than the daily OSRR% of the Gill shield. Increasing rates of daily TSRR% for the shields from the typical grass surface to the white surface were 1.6, 2.3, 1.9, and 1.2, respectively, for the Gill, MMTS, CRS, and ASOS shields (Fig. 6c). Therefore, we anticipate that a snow-covered ground surface (with a surface reflectivity of about 0.85) will increase the interior solar irradiance for the Gill by 1.6 times, the MMTS by 2.3, and the CRS by 1.9, which would act to decouple the temperature sensor from the air temperature. The rank of solar radiation shielding effectiveness, for the whole range of surface solar reflectivity, was ASOS $>$ CRS $\geq$ MMTS $>$ Gill.

The daily TSRR% inside the CRS and MMTS shields was nearly the same, indicating similar shielding efficiency. The Gill shield had larger values, especially at the lower ground surface solar reflectivity. We attribute the high solar shielding effectiveness of the ASOS to the solid sides of the shield.

c. *Temperature difference between shield inner-surface and sensor temperatures*

The difference between the average daytime inner wall surface temperature and the average temperature of the sensor varied from −3° to +4°C (Fig. 7). The temperature difference distribution of each shield follows a Gaussian distribution, with the modes around −0.5°, −0.5°, 0°, and 1°C, and the average values −0.55°, −0.26°, +0.01°, and +0.88°C, respectively, for the Gill, MMTS, CRS, and ASOS shields. The negative average temperature difference for the Gill and MMTS shields reported here is in contrast to other studies that state that the radiation shields could heat the air or air temperature sensor resulting in a shield heating error (e.g., Richardson 1995; Tanner 1990; Tanner et al. 1996). Based on the absolute average difference between the shield inner surface temperature and sensor temperature (Fig. 7), the infrared shielding effectiveness for each shield during daytime was ranked as CRS > MMTS > Gill > ASOS.

During the nighttime, the distribution modes for the difference between the inner-surface temperature of radiation shield and the sensor temperature were approximately zero (Fig. 8). The average values of temperature difference were −0.20°, −0.20°, −0.12°, and −0.07°C, respectively, for the ASOS, CRS, MMTS, and Gill shields. For the MMTS and Gill shields, there were no systematic temperature differences between the inner surface of the radiation shield and the air temperature sensor, as evidenced by the symmetrical shapes of the distributions. The only exception is at a difference of +1°C. The physical basis for this small departure from symmetry has not been determined. The distributions for both ASOS and CRS shields indicate slight skewing toward the infrared cooling effects during the nighttime.

4. Discussion and conclusions

Solar irradiance in the interior of the radiation shield is an important quantity affecting air temperature measurement. Parabolic curves were fit to the fraction of solar radiation entering radiation shields as a function of time of day (Figs. 2, 3, and 5). Although the total solar irradiance ratio TSRR% values were small during midday, the solar irradiance loading on an air temperature sensor installed inside the shield can be relatively large under clear sky conditions, as the absolute interior solar irradiance results from multiplication of the TSRR% and incoming global radiation. Compared to the nonaspirated radiation shields (Gill, MMTS, and CRS), the ASOS shield provided better solar radiation shielding due to its closed cylindrical structure and a relatively large cap (dome) above the shield (Fig. 1). The average TSRR% values inside the shields suggested that the solar radiation shielding effectiveness had the following order: ASOS > CRS > MMTS > Gill. At the normal operating temperature sensor height, the daily TSRR% values inside the Gill, MMTS, and CRS were distinctly different from each other and revealed the same rank in solar radiation shielding effectiveness as for the average TSRR% (Fig. 4).

Although the ASOS is a bottom-open and side-closed shield, the small interior space and black inner surface of the ASOS effectively made it function as a quasi blackbody. The absorbed radiation energy can be partly or completely dissipated by its aspirated airflow. The ASOS performed efficiently as a solar radiation shield above all types of ground surfaces. In addition, the solar radiation shielding effectiveness for the ASOS remained nearly constant from the typical grass surface to the white surface. According to the solar irradiance measurements, the daily TSRR% inside the Gill was larger than that in the CRS and MMTS shields over all types of underlying surfaces (Fig. 6c). The increase of daily TSRR% with increasing underlying surface solar reflectivity was nearly linear for the MMTS, Gill, and CRS shields.

Infrared radiant energy exchange between the shield and the sensor will occur if a temperature difference exists between the two. In contrast to solar radiation effectiveness, the ASOS performed the poorest of the four radiation shields tested on infrared radiation effectiveness during daytime and nighttime conditions (Figs. 7 and 8). The ASOS design allows the air to flow through from the air temperature sensor (bottom portion inside) to the chilled mirror device and past the relatively large heat sink (middle portion inside). The net infrared radiation on the air temperature sensor may heat or cool the air temperature sensor depending on the difference between the inner surface wall temperature and the ASOS sensor temperature and other factors, including ambient solar radiation and dewpoint temperature depression (Fig. 9). The ASOS temperature differences ($T_{\text{inner surface}} - T_{\text{ASOS}}$) generally followed the dewpoint temperature depression rather than the global solar irradiance (Fig. 9). As the dewpoint temperature depression increased, the inner surface temperature surrounding the ASOS temperature sensor became more elevated above the sensor temperature inside the ASOS. In contrast, the decrease in dewpoint temperature depressions generally led to a lower heat generation rate of chilled mirror system. In addition, the large size of the chilled mirror system located in the middle portion of the ASOS shield greatly reduced airspeed past the PRT sensor, which is located in a wake zone. The airflow rate through the PRT sensor did not reach as high as the initial airflow rate at the entrance of the ASOS shield (around 2.6–3.2 m s^{-1} measured by a hot-wire ane-

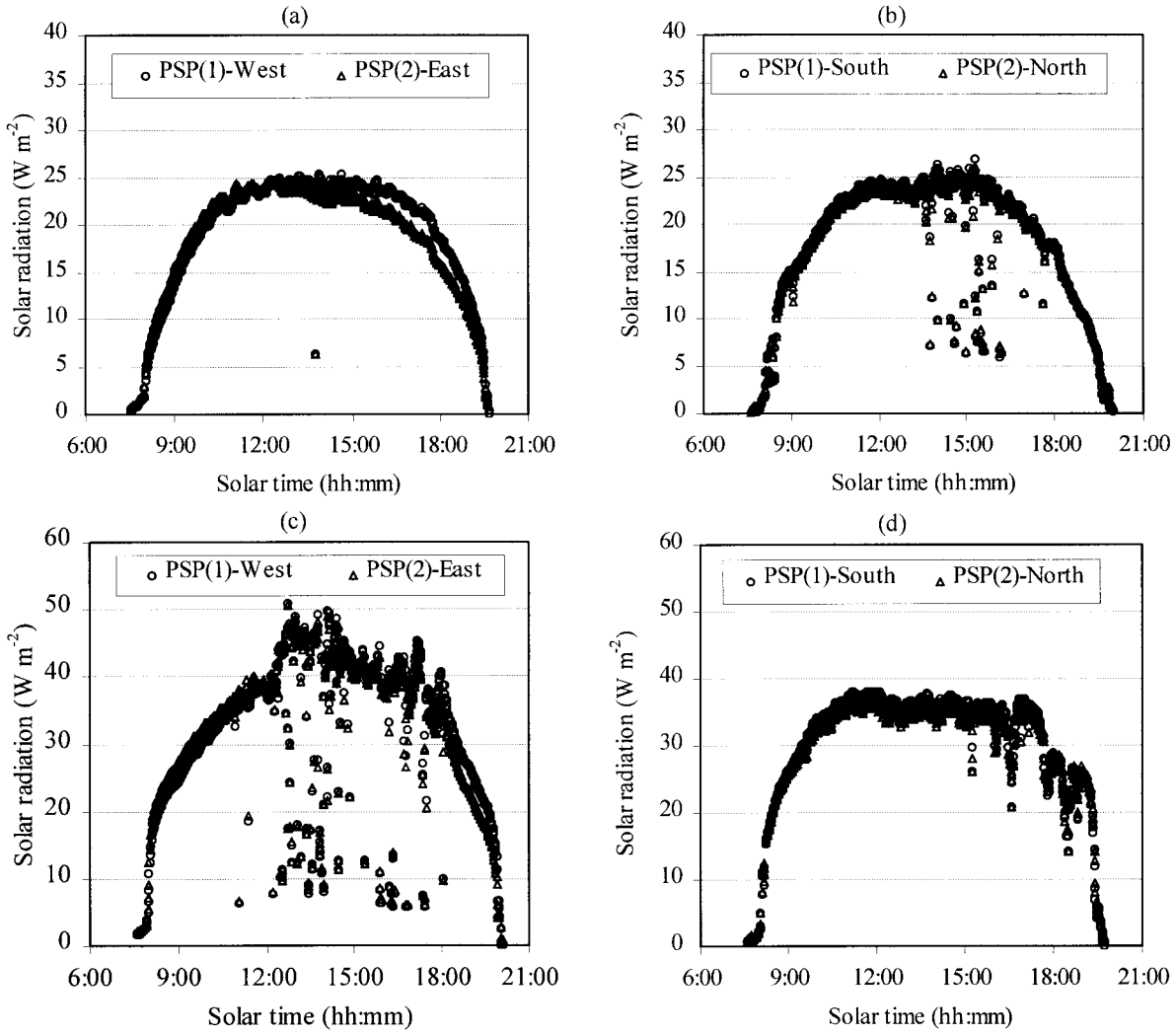

FIG. A1. Solar irradiance inside the CRS shield and the Big Shield using two PSP pyranometers in 1999. (a) PSP east–west orientation inside the CRS shield at DOY 245. (b) PSP south–north orientation inside the CRS shield at DOY 244. (c) PSP east–west orientation inside the Big Shield at DOY 236. (d) PSP south–north orientation inside the Big-Shield at DOY240.

mometer). Therefore, the chilled mirror system including the heat sink is a major contributor to infrared radiation heating or cooling errors on the air temperature sensor.

Statistical distribution of the temperature difference between the inner surface and the sensor temperatures inside the CRS shield was centered around zero for both daytime and nighttime conditions (Figs. 7 and 8) but average -0.2°C temperature difference for nighttime. The Gill and MMTS shields were most likely to cause an infrared radiation deficit for the sensor during daytime. According to heat transfer considerations, heating or cooling effects are not only dependent on the surface temperatures but also on surface emissivities. Therefore, a surface with a high temperature does not necessarily transfer all its energy onto the surface with low temperature. However, the infrared radiation effect on the sensor temperatures for the MMTS and Gill shields during daytime caused a slight lowering of the sensor temperature if the inner-surface and sensor emissivities are the same. The slight cooling effects would cancel out part of the solar radiation heating effects inside the MMTS and Gill shields. There were no obvious temperature difference trends toward positive or negative for the MMTS and Gill shields during nighttime (Fig. 8). The rank of the infrared radiation shielding effectiveness was CRS $>$ MMTS $>$ Gill $>$ ASOS during daytime and Gill $\geq$ MMTS $>$ CRS $\approx$ ASOS during nighttime, based on the absolute magnitude of average temperature difference values for each shield. Tanner et al. (1996) noted cooling effects in the shields during nighttime but their results (their Fig. 8) show both cooling and heating, because the temperature errors were distributed evenly around zero for the Gill shield during nighttime. This is consistent with our results (Fig. 8).

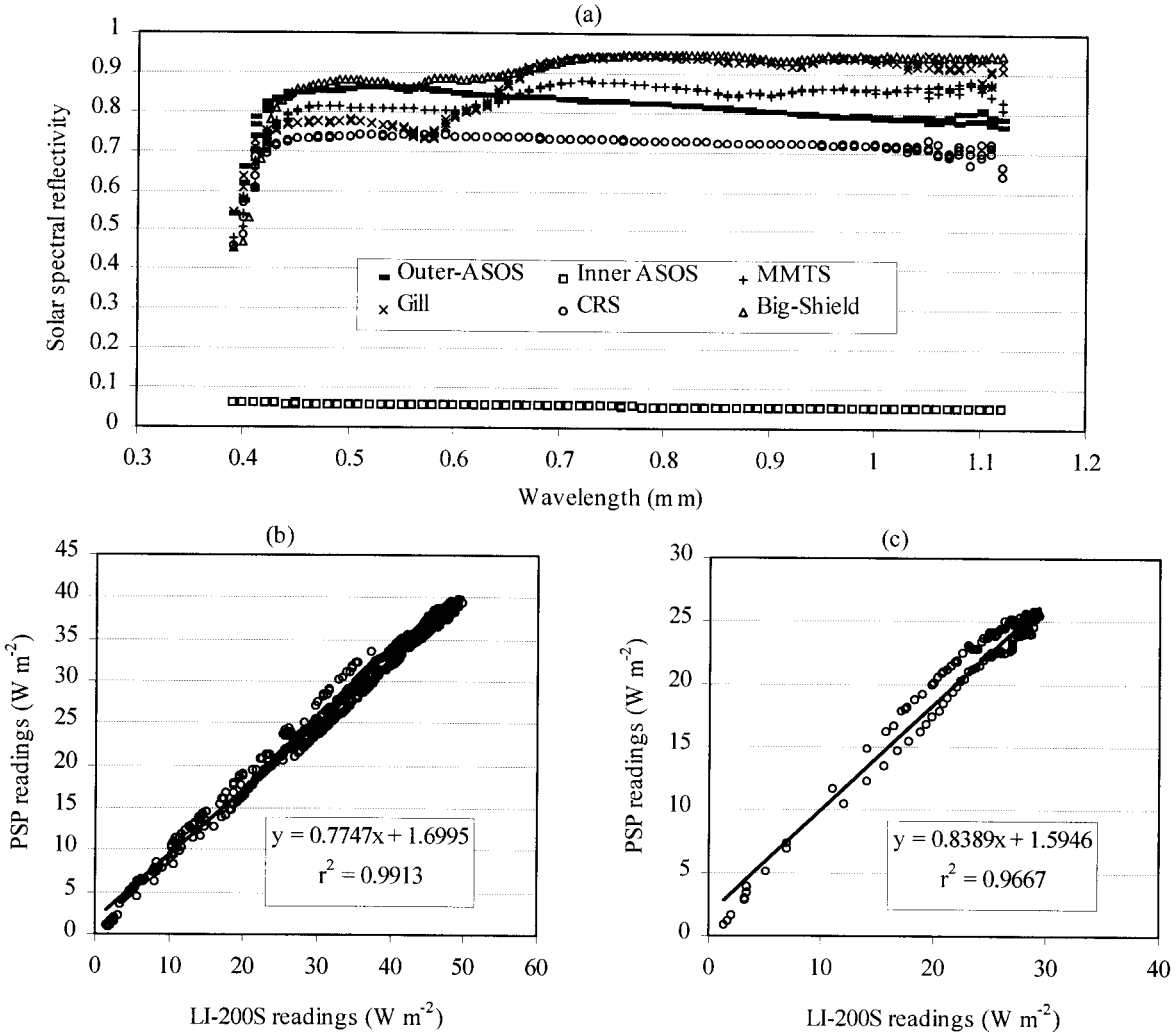

FIG. A2. (a) Shield surface spectral reflectivity. (b) In situ LI-200S calibration inside the Big Shield for the MMTS and Gill shields. (c) In situ LI-200S calibration inside the CRS shield.

Acknowledgments. We are grateful to Vickie L. Nadolski (NWS) and Tom Blackburn (NWS) for the loan of two ASOS and two MMTS temperature systems. Comments on a draft of this paper by Drs. James R. Brandle and George E. Meyer are gratefully acknowledged. We also thank Drs. Albert Weiss and Steve J. Meyer for the internal review of the original manuscript.

APPENDIX

Validation of LI-200S Pyranometer

The LI-200S pyranometer is ideal for this experiment because of its small size, which allows it to fit inside all four radiation shields. However, due to the specific spectral response characteristics of the sensing element (photodiode), the LI-200S sensor must be calibrated when placed in a new spectral environment (LI-COR, Inc. 1991). To accomplish this, we developed a big multiple-plate radiation shield (Big-Shield) at a scale 3.5 times the dimension of the original MMTS shield. The Big-Shield was made of white PVC plates similar to the material from which the Gill and MMTS shields are constructed. This large enclosure could house two Eppley precision spectral pyranometers (PSPs), which measure the solar irradiance with a full spectral response. The Big-Shield was used to calibrate the LI-200S for conditions to be encountered inside the two multiple-plate shields: the Gill and MMTS shields. The solar spectral reflectivity of all surfaces of the radiation shields (ASOS, MMTS, Gill, CRS, and Big-Shield) was measured using an SE590 spectrometer (Spectron Engineering Inc., Denver, Colorado). The measurements of solar spectral reflectivities of the shield surfaces indicated that the MMTS, Gill, and Big-Shield plates had similar solar spectral distribution within the 0.4–1.1-μm wavelength region. Therefore, the Big-Shield was accepted as a surrogate for the Gill and MMTS shields in this particular calibration application.

Figure A1 gives the solar irradiance distribution inside the CRS shield and the Big-Shield using two PSPs set side by side under clear or mostly clear sky conditions. The solar irradiance inside these two shields was uniformly distributed (Fig. A1) regardless of the orientations of two PSPs inside the CRS shield and the Big-Shield. This result made it possible to calibrate an LI-200S by comparison to an adjacent PSP inside the CRS or the Big-Shield. The calibration of the LI-200S within each shield gave a linear regression equation for each shield (Fig. A2). These calibration equations were applied to LI-200S data when the LI-200S was used for measuring solar irradiance inside the MMTS, Gill, and CRS shields.

REFERENCES

Brock, F. V., J. Richardson, and S. R. Semmer, 1995: Passive multiplate solar radiation shields. Preprints, *Ninth Symp. on Meteorological Observations and Instrumentation*, Charlotte, NC, Amer. Meteor. Soc., 179–183.

Fuchs, M., and C. B. Tanner, 1965: Radiation shields for air temperature thermometers. *J. Appl. Meteor.*, **4,** 544–547.

Gill, G. C., 1979: Development of a small radiation shield for air temperature measurements on drifting buoys. NOAA Rep. Contract 01-7-038-827, National Data Buoy Center, Stennis Space Center, MS, 23 pp.

——, 1983: Comparison testing of selected naturally ventilated solar radiation shields. NOAA Rep. Contract NA-82-0A-A-266, Stennis Space Center, MS, 15 pp.

Guttman, N. B., and C. B. Baker, 1996: Exploratory analysis of the difference between temperature observations recorded by ASOS and conventional methods. *Bull. Amer. Meteor. Soc.*, **77,** 2865–2873.

Hart Scientific, Inc., 1996: Model 5627 industrial RTD probe user's guide. Hart Scientific Inc., 20 pp.

LI-COR, Inc., 1991: *LI-COR Radiation Sensors Instruction Manual.* Revised ed. LI-COR, Inc., 24 pp.

Lin, X., and K. G. Hubbard, 1999: Microclimate inside air temperature radiation shields. High Plains Climate Center (HPCC) Rep. 99-1 to National Weather Service, University of Nebraska—Lincoln, 187 pp.

McKay, D. J., and J. D. McTaggart-Cowan, 1977: An intercomparison of radiation shields for auto stations. *Proc. World Meteorological Organization (WMO) Conf.*, Geneva, Switzerland, WMO, 208–213.

Meteorological Office, 1965: Handbook of meteorological instruments. Part I: Instruments for surface observations. Her Majesty's Stationery Office, 458 pp.

Monteith, J. L., and M. H. Unsworth, 1990: *Principles of Environmental Physics.* 2d ed. Edward Aenold, 291 pp.

Richardson, S. J., 1995: Multiplate radiation shields: Investigating radiational heating errors. Ph.D. thesis, University of Oklahoma, 133 pp.

Tanner, B. D., 1990: Automated weather stations. *Remote Sens. Rev.*, **5** (1), 73–98.

——, E. Swiatek, and C. Maughan, 1996: Field comparisons of naturally ventilated and aspirated radiation shields for weather station air temperature measurements. Preprints, *22d Conf. on Agricultural and Forest Meteorology*, Atlanta, GA, Amer. Meteor. Soc., 227–230.

Wendland, W. M., and W. Armstrong, 1993: Comparison of maximum–minimum resistance and liquid-in-glass thermometer records. *J. Atmos. Oceanic Technol.*, **10,** 233–237.

Wylie, R. G., and T. Lalas, 1992: Measurement of temperature and humidity: Specification, construction, properties and use of the WMO reference psychrometer. WMO Rep. 759, 71 pp.